ACS OMEGA

http://pubs.acs.org/journal/acsodf

Article

Label-Free Detection and Characterization of Heparin-Induced Thrombocytopenia (HIT)-like Antibodies

Nida Zaman Khan, Li-Yu Chen, Annerose Lindenbauer, Uwe Pliquett, Holger Rothe, and Thi-Huong Nguyen*

Cite This: *ACS Omega* 2021, 6, 25926−25939

Read Online

ACCESS | Metrics & More | Article Recommendations

ABSTRACT: Heparin-induced thrombocytopenia (HIT) antibodies (Abs) can mediate and activate blood cells, forming blood clots. To detect HIT Abs, immunological assays with high sensitivity (≥95%) and fast response are widely used, but only about 50% of these tests are accurate as non-HIT Abs also bind to the same antigens. We aim to develop biosensor-based electrical detection to better differentiate HIT-like from non-HIT-like Abs. As a proof of principle, we tested with two types of commercially available monoclonal Abs including KKO (inducing HIT) and RTO (noninducing HIT). Platelet factor 4/Heparin antigens were immobilized on gold electrodes, and binding of antibodies on the chips was detected based on the change in the charge transfer resistance (R_{ct}). Binding of KKO on sensors yielded a significantly lower charge transfer resistance than that of RTO. Bound antibodies and their binding characteristics on the sensors were confirmed and characterized by complementary techniques. Analysis of thermal kinetics showed that RTO bonds are more stable than those of KKO, whereas KKO exhibited a higher negative ζ potential than RTO. These different characteristics made it possible to electrically differentiate these two types of antibodies. Our study opens a new avenue for the development of sensors for better detection of pathogenic Abs in HIT patients.

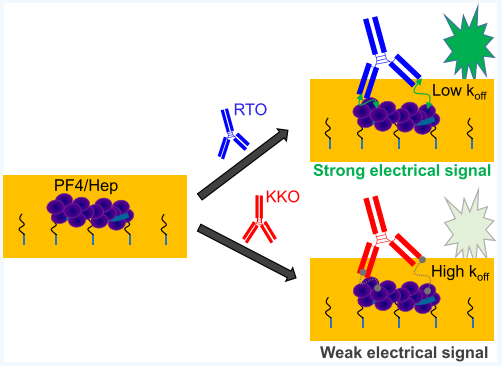

INTRODUCTION

Heparin discovered in 1916 plays an important role in many biological processes[1] such as viral/bacterial infections,[2,3] angiogenesis,[4] inflammation,[5] cancer metastasis,[6] and anticoagulation.[7] However, up to 5% of the patients with heparin administration suffer from heparin-induced thrombocytopenia (HIT), which can cause life-threatening complications.[8] The heparin (H) binds electrostatically to platelet factor 4 (PF4), forming an antigenic PF4/H complex leading to the formation of anti-PF4/H antibodies (aPF4/H Abs). Some of these antibodies bind to the FcγRIIa receptor and activate platelets.[9,10] This triggers a cascade of accumulation of multiple blood cells and plasma proteins. The pathophysiological outcome is thrombosis/thrombocytopenia, gangrene, and limb ischemia, which is associated with a loss of platelet count of more than 50%,[11,12] and a mortality rate up to 30%.[13] It has been reported that 600 000 people per year develop HIT, which is double the number of breast cancer cases diagnosed annually in the US (US Cancer Statistics Working Group), and nearly equal to the number of new cases of angina diagnosed each year.[14]

In severe Covid-19 patients, heparin is recommended for the management of coagulopathy[15] as they appear to be associated with a better prognosis.[16,17] However, HIT Abs were detected frequently in Covid-19 patients[18] with a higher incidence than in non-Covid patients.[19] Pathogenic antibodies caused the worst clotting in Covid-19 patients.[20] Early detection of HIT antibodies is important so that heparin therapy can be stopped as failure to diagnose HIT can lead to catastrophic thrombosis if heparin therapy is continued. Therefore, a quick and accurate diagnosis of HIT must be made in case it occurs, especially in Covid-19 patients.

To date, the detection of these antibodies, however, is still challenging. Because of their high sensitivity and fast response, enzyme-linked immunosorbent assay (ELISA) testing with human plasma is widely used to detect anti-PF4/Heparin antibodies that bind to PF4/Heparin antigens coated on ELISA plates. However, only 50% of ELISA results define pathogenic HIT.[21] The incorrect prediction of HIT leads to the wrong decision of the doctor to treat patients. Unnecessary treatment for HIT in patients without HIT problems can cause serious consequences such as venous limb gangrene or fatal hemorrhage.[22] To improve detection, functional assays such as

Received: May 13, 2021
Accepted: September 16, 2021
Published: September 29, 2021

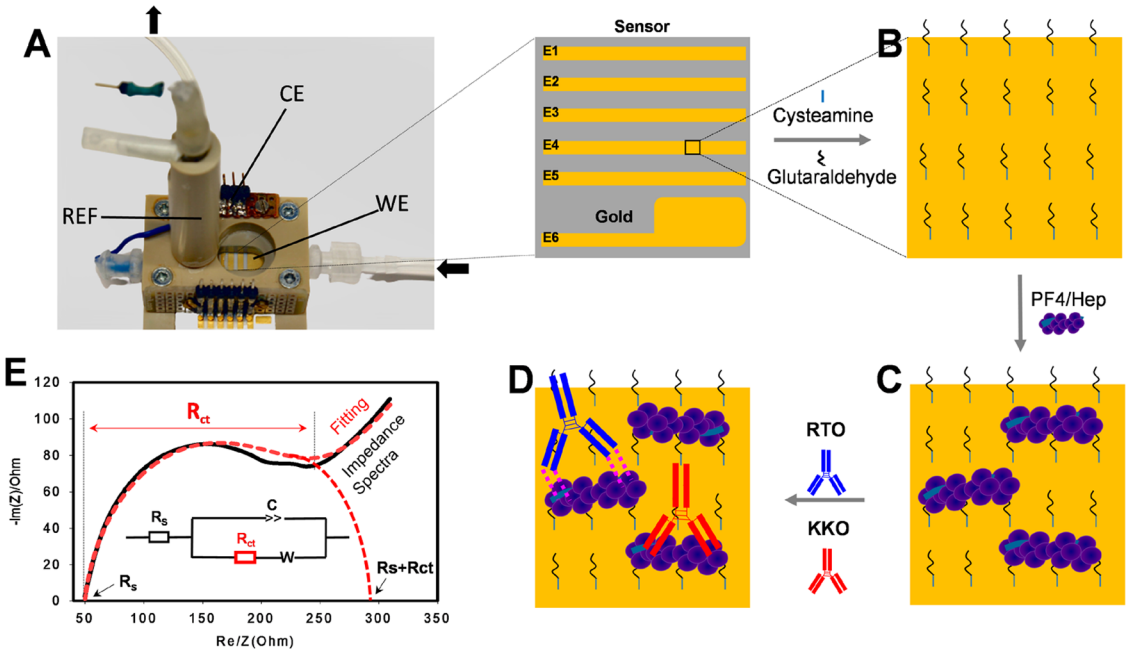

Figure 1. Schematic illustration of the biosensor for detection of HIT-like antibodies. (A) EIS chamber used for impedance measurement consists of a reference electrode (REF), a working electrode (WE or sensor), a counter electrode (CE), input, and output (arrows) channels. The sensor comprising five electrodes of the same size (E1−E5) (yellow) were used while the large electrode (E6) was excluded. (B) Self-assembled monolayer (SAM) was formed by thiol−Au covalent bonds between cysteamine and the gold surface while glutaraldehyde was linked to cysteamine, allowing binding of (C) PF4/H complexes. (D) Added antibodies such as RTO (blue) or KKO (red) bind to the sensor *via* PF4/H complexes. (E) Typical Nyquist diagram (black) and Z-Fit (red) allowed determination of R_{ct} as well as R_s, W, and C. (Inset in E) Most suitable circuit model for the interpretation of the measured impedance spectra.

the serotonin release assay (SRA)[23] or heparin-induced platelet aggregation tests (HIPA)[24] are additionally recommended to confirm ELISA positive results. These assays provide specificity of ∼90%. However, functional assays require fresh platelets isolated from healthy human blood, which is not available in every laboratory. Therefore, numerous physicians must rely on the results of immunoassays or suspected samples must be sent to other laboratories for confirmatory tests.

A rapid HIT test is commercially available since 2004, however, it did not reveal useful diagnostic information for the detection of HIT antibodies.[25] Recently, tests with high diagnostic accuracy and good reproducibilities such as a rapid particle gel immunoassay (PaGIA) or IgG-specific chemiluminescence immunoassay (AcuStar HIT-IgG) have been developed.[26,27] Still, the results from these tests must also be confirmed in other settings and larger populations.[28] Other methods such as quartz crystal microbalance with dissipation[29] or impedance spectroscopy[30] have been investigated, but these tests are based on the principle of functional tests in which fresh blood samples are required.

Recently, we found that single-molecule force spectroscopy (SMFS)-based atomic force microscopy (AFM) allows us to differentiate between pathogenic and nonpathogenic aPF4/H Abs.[31−34] The SMFS technique has become an important tool to study biomolecular interactions as it allows direct measurements of the bond dynamics and kinetic properties of interactions in different living conditions. It provides information that could not be assessed by other bulk experiments.[35,36] The resolution of the SMFS techniques can reach a range of angstrom in length and piconewton in force (5 pN−100 nN).[37] However, SMFS is an expensive, time-consuming technique that requires experienced operators and data analysis. Thus, it only allows us to unravel fundamental characteristics of aPF4/H Abs, but it has not yet been designed as a diagnostic tool for clinical laboratories. Nevertheless, these findings proved that aPF4/H Abs are qualitatively different, i.e., the pathogenic aPF4/H Abs show stronger binding strength, higher binding energy, more stable bonds, and different binding epitopes as compared with the non-pathogenic ones when interacting with the same PF4/H complexes. We hypothesize that these different binding characteristics of HIT antibodies could be electrically detected.

In this study, we established as a proof of principle an impedimetric biosensor to distinguish between pathogenic and nonpathogenic aPF4/H Abs by electrochemical impedance spectroscopy (EIS). EIS allows label-free detection of the bound antibodies on the sensors through the change of the charge transfer resistance (R_{ct}) at the biofunctionalized electrode/biological liquid interface. The deposition of molecules can block or facilitate charge transfer into the electrode of the sensor. In both ELISA and EIS experiments, PF4/H complexes are coated on the plate or the sensor for capturing HIT Abs. However, both HIT and non-HIT Abs are detected in ELISA by the optical density generated from the secondary enzyme-conjugated antibody. As the aPF4/H Abs are intrinsically different,[31−34] we suspect that their binding characteristics differ electrically, which are detectable using EIS. Taking the influence of the charge transfer at the interface between the biofunctionalized electrode and biological material into account, the charge transfer resistance R_{ct} should be most sensitive to the binding of different antibodies. A suitable model for this interface is the Randles circuit where the charge transfer resistance R_{ct} signifies the resistance of electron transfer when layers are added on the gold electrode.[38,39]

As a proof of principle, we tested in this study with two types of commercially available well-characterized monoclonal HIT-

https://doi.org/10.1021/acsomega.1c02496
ACS Omega 2021, 6, 25926−25939

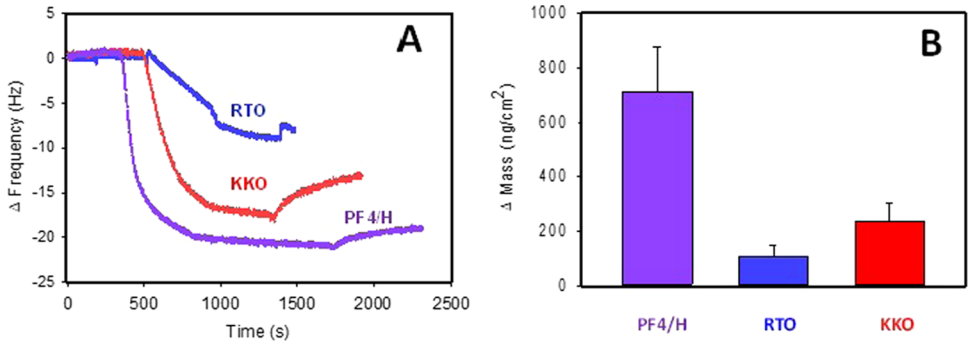

Figure 2. Binding of antibodies on the sensor induced mass changes detected by QCM. (A) RTO (blue) induced lower frequency changes, indicating a lower bound mass on the chip than the KKO (red), while bound PF4/H complexes exhibited the highest bound mass. The ending saturated parts on PF4/H complex curves are considered as the zero frequency in measurements of RTO and KKO. (B) Frequency shifts are converted to mass changes. The average and corresponding standard deviation showed the highest mass for (violet) PF4/H complexes, followed by (red) KKO, and the lowest for (blue) RTO (n = 3 repetitions).

like murine aPF4/H Abs including RTO and KKO. It has been shown that RTO[40] has binding characteristics similar to the non-HIT aPF4/H Abs, while KKO[41−43] mimics the HIT antibodies. The main difference is, although both RTO and KKO bind to PF4/H complexes, KKO bridges/activates platelets *via* FcγRIIa and induces HIT, whereas RTO does not.

Here, we immobilized PF4/H antigens on gold electrodes and added RTO or KKO for binding. The change in charge transfer resistance R_{ct} due to antibody binding was detectable by EIS. Additionally, the mass added to the sensor was quantified by quartz crystal microbalance (QCM) measurements. Moreover, the binding was visualized by confocal laser scanning microscopy (CLSM) by means of immunofluorescence staining. Insights into molecular interactions due to binding were obtained by single-molecule force spectroscopy (SMFS) and dynamic light scattering (DLS). Our results showed a distinct binding of both RTO and KKO on the surfaces coated with PF4/H complexes. KKO yielded a significantly lower charge transfer resistance than RTO, indicating that antibodies with dissimilar binding characteristics could be distinguished employing electrical characterization. As currently available methods for detection of HIT involve either low accuracy, molecular labeling, or fresh blood, the fast and label-free EIS technique with femtogram possible detection is a promising method for the future development of biosensors for better detection of HIT.

RESULTS

Biosensor for Detection of HIT Antibodies. The electrochemical impedance spectroscopy (EIS) setup is composed of a working electrode (WE) (i.e., the area where the reaction of interest occurs) and the reference electrode (Ref) (i.e., a potential control), while the counter electrode (CE) serves as a current injecting electrode for circuit closure (Figure 1A). The current flows in between the working electrode and the counter electrode while the reference electrode only monitors the potential of the working electrode for the control feedback.

The five working electrodes E1−E5 (Figure 1A) were coated with cysteamine which was then linked to glutaraldehyde (Figure 1B). Preformed PF4/H complexes were covalently linked to glutaraldehyde (Figure 1C). The antibodies added to the sensor bound to PF4/H complexes (Figure 1D).

A typical Nyquist diagram obtained by EIS (black, Figure 1E) and the fitting of the spectrum with Z-fit analysis (red, Figure 1E) allows the determination of impedance parameters such as solution resistance (R_s), the Warburg element (W) as the diffusion element, constant phase element (C), and the charge transfer resistance (R_{ct}). In our experiments and also as described in the previous study,[44] the R_{ct} was most sensitive compared to other parameters when proteins were added. Therefore, R_{ct} was chosen to differentiate the binding between RTO and KKO.

Binding of HIT Antibodies on the Sensor. Before investigating the binding of antibodies on the sensor by electrochemical impedance spectroscopy, we confirmed that both PF4/H complexes and antibodies bind to the sensor. The mass changes due to protein binding were first quantified by quartz crystal microbalance (QCM) and then visualized by immunofluorescence detection using confocal laser scanning microscopy (CLSM).

Mass Detection in Quartz Crystal Microbalance (QCM). As QCM experiments also detect the binding of target molecules on a Au-sensor but with different principles than EIS, we used QCM as a complementary technique to quantify our successful immobilization of proteins on the sensor. QCM is a label-free technique utilizing the quartz piezo crystal, which vibrates at the resonance frequency. Additional mass on the sensor induces a detectable shift in the resonant frequency and dissipation factor, which is determined in comparison to a clean quartz crystal. The shift in the resonant frequency exhibits a linear dependence with the addition of mass as long as the added mass is below 0.5% of the mass of the crystal. This relationship is governed by the Sauerbrey equation.[45] We first tested whether both RTO and KKO bind to the QCM sensor by detecting mass changes. For that, we coated the chip first with PF4/H complexes before adding RTO or KKO for binding. The plateau of frequency at approximately zero (Figure 2A) was considered as the baseline in which PF4/H complexes have already bound with a change in a frequency shift of about 23 Hz that corresponds to a mass change of 713 ± 165 ng/cm^2 (Figure 2B). When adding RTO (blue) or KKO (red), the frequency shift was reduced to approximately 10 or 18 Hz, respectively (Figure 2A). The changes in mass due to the binding of RTO or KKO were determined using Sauerbrey eq 1,[45]

$$\Delta m = -S_{QCM} \times \Delta f \quad (1)$$

where, Δm is the mass change, Δf is the frequency shift, and S_{QCM} is the mass sensitivity constant (Sauerbrey-constant),

https://doi.org/10.1021/acsomega.1c02496
ACS Omega 2021, 6, 25926−25939

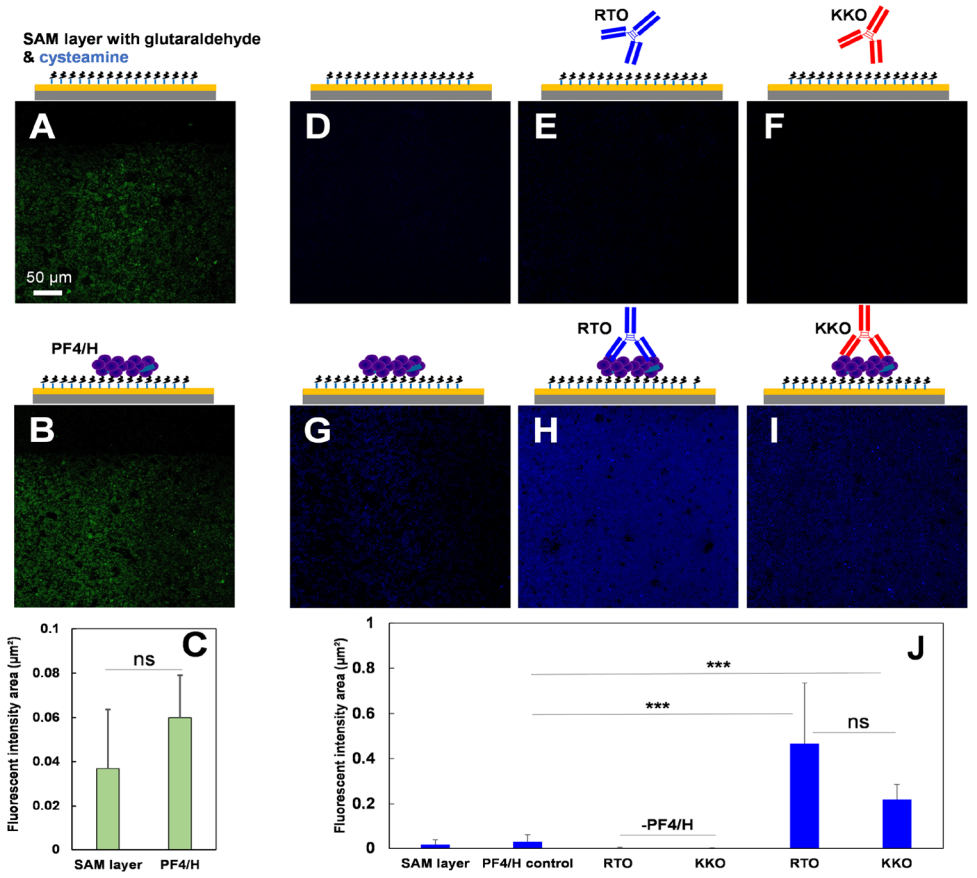

Figure 3. Visualization of binding of PF4/H complexes and antibodies on the sensors. (A–C) Fluorescent-labeled anti-PF4 FITC antibodies were incubated on the SAM layer and (B) with PF4/H complexes. (C) Bound PF4/H complexes showed a higher fluorescence intensity than the SAM layer, indicating binding of PF4/H complexes on the sensor. (D–I) Fluorescent-labeled anti-mouse Alexa 488 antibodies were incubated on (D) SAM layer, (E) SAM layer with RTO, or (F) KKO in the absence of PF4/H complexes, (G) PF4/H complexes, (H) RTO, or (I) KKO on PF4/H complexes. (J) Average values and standard deviations of the fluorescence intensity showed more binding of RTO than KKO while the controls showed a minimal signal. Note: Black areas in CLSM images (top, A, B) are surfaces without Au layers; scale bar applies for all images. n = 2–3 repetitions; *** = significant difference ($P < 0.001$) and ns = no significant difference ($P > 0.05$).

which has a standard value of 17.7 ng/cm^2 for 5 MHz of crystal. The average mass difference and corresponding standard deviation from different measurements showed higher mass changes induced by binding of KKO compared to RTO, while PF4/H complexes alone bound strongly to the chip shown as the highest accumulated mass changes (Figure 2B).

Immunofluorescence Detection of Bound Proteins on the Sensor by Confocal Laser Scanning Microscopy (CLSM). Bound proteins on the sensors were further visualized by immunofluorescence detection utilizing confocal laser scanning microscopy (CLSM). Here, the immobilization of proteins on the sensors was prepared following the standard protocol for EIS experiments. To visualize bound PF4/H complexes, anti-PF4 FITC-labeled antibodies were incubated with the sensor after self-assembled monolayer (SAM) deposition (including cysteamine, glutaraldehyde, and surface blockage with ethanolamine) (Figure 3A) with subsequent coating with PF4/H complexes (Figure 3B). Quantification of the fluorescence intensity showed a higher signal on PF4/H complexes than on the SAM layer, indicating binding of PF4/H complexes on the sensors (Figure 3C). However, using the anti-PF4 FITC antibody, the fluorescence signal was weak as no significant difference in signal between PF4/H complexes and the SAM layer was observed. We attributed that heparin induced changes in the conformation of PF4, as previously described,[46] and therefore, a reduction of binding of the anti-PF4 FITC antibody to PF4/H complexes was seen. Nevertheless, these results together with QCM data indicated that the PF4/H complexes were immobilized on the EIS sensors.

To visualize HIT antibodies binding, PF4/H complex-coated sensors were incubated with either RTO or KKO before incubating with the anti-mouse IgG Alexa 488 antibody. CLSM images showed some minor binding of the anti-mouse IgG Alexa 488 antibody on the SAM layer (Figure 3D), RTO (Figure 3E), and KKO (Figure 3F) in the absence of PF4/H complexes. Some weak signals were obtained on PF4/H complexes (Figure 3G) and a strong signal was observed when RTO (Figure 3H) or KKO (Figure 3I) was incubated on PF4/H complexes. Quantification of fluorescence signal areas showed stronger binding of RTO than KKO and both antibodies showed a significantly higher signal than that on the sensor coated with the PF4/H complex, while other controls showed a minimal signal (Figure 3J). The results indicated that both RTO and KKO were bound to PF4/H complexes immobilized at the sensors.

Detection of HIT Antibodies by Electrochemical Impedance Spectroscopy (EIS). After binding of PF4/H complexes, RTO and KKO on the sensors were confirmed, and we next detected their binding by means of EIS. The procedure for sample preparation and the principle of EIS

https://doi.org/10.1021/acsomega.1c02496
ACS Omega 2021, 6, 25926–25939

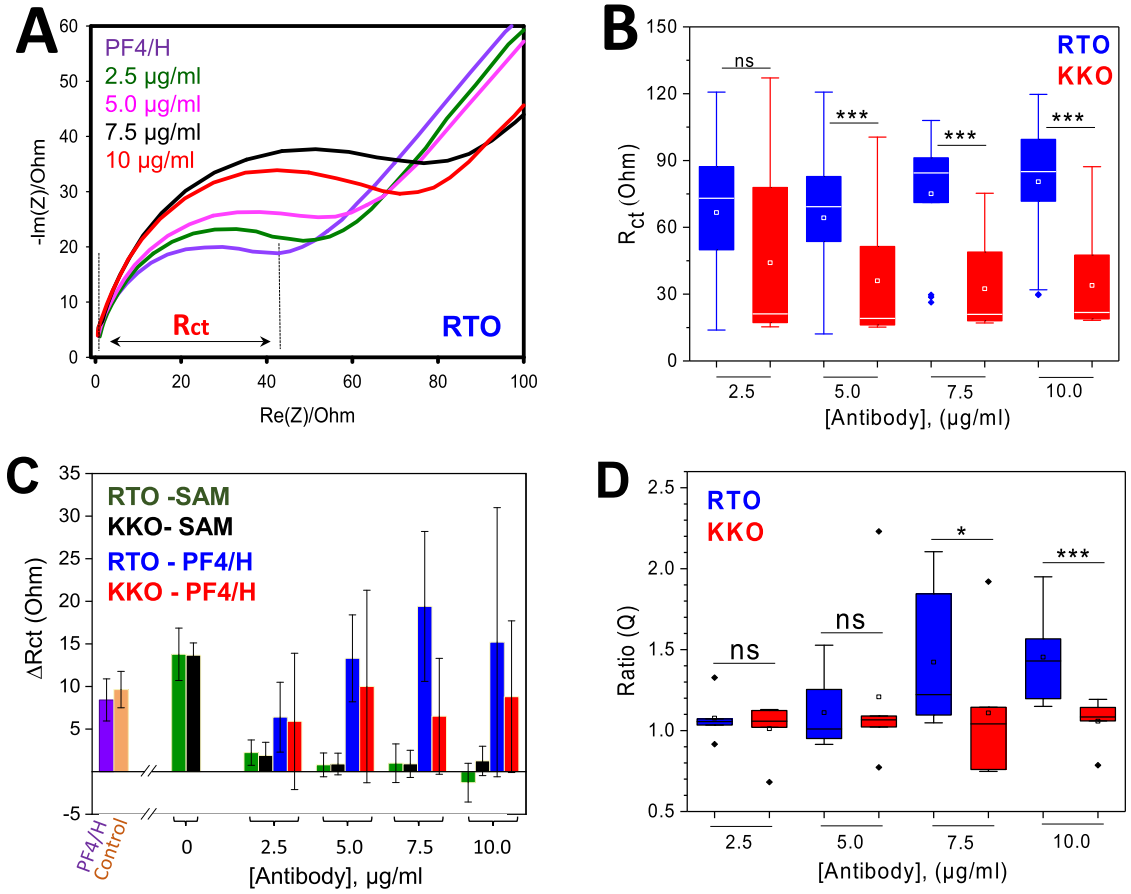

Figure 4. Detection of the HIT antibody by EIS. (A) Example of measured Nyquist diagrams obtained by EIS showing different spectra measured with PF4/H complexes (violet) and RTO at concentrations of 2.5 μg/mL (green), 5 μg/mL (pink), 7.5 μg/mL (black), and 10 μg/mL (red). The spectra developed while the R_{ct} increased with increasing RTO concentration. (B) R_{ct} induced by RTO binding (13 electrodes) is significantly higher than that of KKO (10 electrodes) tested by one-way ANOVA tests (analysis of variance). (C) Average $\Delta R_{ct} \pm$ SD subtracted from the glycine cycle showed higher values for RTO (blue) than for KKO (red) at $\geq$5 μg/mL while the minimal signal was observed when RTO (green) or KKO (black) interacted with SAM layers in the absence of PF4/H. Control human antibodies (yellow, C) do not bind to PF4/H complexes showing a similar ΔR_{ct} value as compared with PF4/H alone (violet, C) coated on the sensor. (D) Ratio Q shows a significant difference between RTO and KKO at $\geq$7.5 μg/mL. Statistics were obtained by one-way ANOVA test, *** = significant difference, * = difference, and ns = no significant difference ($P > 0.05$).

are similar to those for QCM. However, the detection principle is quite different, in EIS measurements, the change in charge transfer resistance (R_{ct}) due to molecules adhering to the sensor is detected. All electrodes of the sensor were coated first with PF4/H complexes, and then RTO or KKO from 2.5 to 10 μg/mL were added for binding. The EIS measurements were carried out first for the bare sensor, followed by the PF4/H complex-coated sensor, and lastly for antibodies of different concentrations added. Before adding the next concentration, the bound antibodies on the sensor at the previous concentration were removed with 100 mM glycine. After rinsing with electrolyte buffer ($Fe(CN)_6^{3-/4-}$), EIS measurements were again recorded, shown as Nyquist diagrams as an example for RTO (Figure 4A). Adding RTO at 2.5 μg/mL to PF4/H complexes to the sensor caused the development of the spectra and increased further with a higher RTO concentration (Figure 4A). However, the 7.5 μg/mL concentration provided the highest detection signal. At 10 μg/mL, impedance is lower than at 7.5 μg/mL. We attributed that a saturation binding of antibodies on the sensor was reached at 7.5 μg/mL. At the higher concentration (10 μg/mL), either binding competition among antibodies occurred or the system reached a detection limit that led to a reduction of the impedance signal. The spectra were then fitted to the Randles circuit using Z-fit analysis, which allowed the determination of charge transfer resistance (R_{ct}).

To quantify the difference of charge transfer resistance between RTO and KKO, we analyzed results from 13 different electrodes for RTO and 11 electrodes for KKO at various antibody concentrations for statistical comparison. The results showed a significant difference in the measured R_{ct} between RTO and KKO at the $\geq$ 5 μg/mL concentration (Figure 4B), indicating a dissimilar binding between KKO and RTO on the sensors. To obtain more accurate changes, we subtracted the signal of antibody binding from the baseline at the glycine step before adding antibodies of each concentration, i.e., the difference in charge transfer resistance: $\Delta R_{ct} = R_{ct}(\text{antibody}) - R_{ct}(\text{glycine})$. The average $\Delta R_{ct} \pm$ SD is higher for RTO compared to KKO at all antibody concentrations (Figure 4C), which are significantly higher than the signal obtained when RTO or KKO interacted with SAM layers. This ΔR_{ct} also increased with increasing antibody concentration but RTO showed a stronger increase in ΔR_{ct} than KKO (Figure 4C). Human sera containing antibodies that do not bind to PF4/H complexes in ELISA and do not induce platelet activation were used as the control. We tested with a 1:200 dilution following

https://doi.org/10.1021/acsomega.1c02496
ACS Omega 2021, 6, 25926−25939

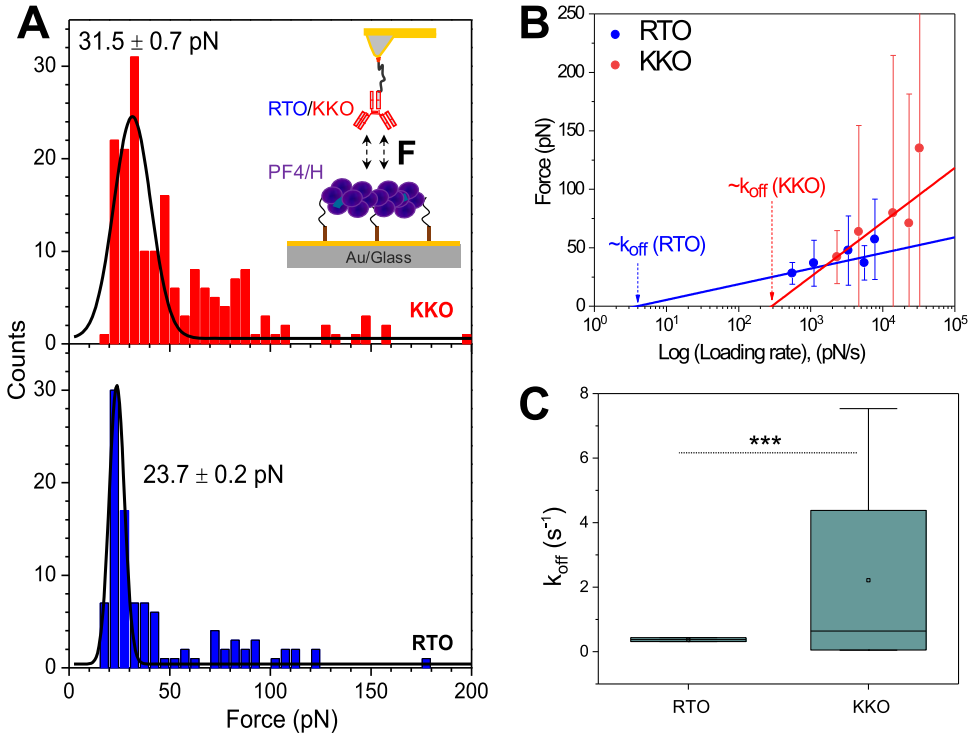

Figure 5. Binding characteristics of RTO and KKO to PF4/H complexes determined by SMFS. (A) Single RTO or KKO was linked covalently to the AFM-tip *via* PEG linkers, and PF4/H complexes were immobilized on the substrate for the measurement of their interaction force F. (A) Rupture forces and the corresponding standard errors determined by a Gaussian fit (solid curves) are lower for (blue) RTO than for (red) KKO. (B) Plot of rupture forces against different logarithmic loading rates allowed us to determine the relative thermal off-rate ($\sim k_{off}$) at $F = 0$ of the interactions. (C) KKO ($n = 4$ repetitions) shows significantly higher k_{off} than RTO ($n = 3$ repetitions) and *** = significant difference in the ANOVA test.

the standard protocol described in the ELISA test with patient sera.[47] The diluted sera were added to the sensor coated with the PF4/H antigen. This control showed a relatively similar ΔR_{ct} value as compared with ΔR_{ct} obtained for the PF4/H antigen alone, indicating no binding of control antibodies to the PF4/H antigen-coated sensor (Figure 4C).

However, large variations at each concentration were observed by analyzing average $\Delta R_{ct} \pm$ SD obtained from different electrodes. Perhaps, the number of bound antibodies on the sensor varied, depending on the density of the PF4/H complexes coated on the sensors. The amount of bound PF4/H complexes on the sensor has a strong correlation with the dimension of the electrodes. We found that an average of 12 electrodes has a width of 1.50 ± 0.03 mm and a length of 7.06 ± 0.06 mm. This variation of approximately 30 μm in width and 60 μm in length within electrodes led to an unequal amount of antigens and antibodies coated on each electrode. Therefore, an average ΔR_{ct} from different electrodes and sensors resulted in large deviations. Thus, a comparison of the charge transfer resistance measured among electrodes may not be accurate. We, therefore, established a ratio (Q) between R_{ct} measured at each antibody concentration and the R_{ct} measured on PF4/H complexes (eq 2). The Q-value represents the binding of antibodies per unit PF4/H complexes.

$$Q = \frac{R_{ct}(\text{abs})}{R_{ct}(\text{PF4/H})} \tag{2}$$

By this calculation, we found a stronger increase of RTO binding per unit PF4/H complex than that of KKO (Figure 4D). The Q-value did not show a significant difference between the two types of antibodies at the ≤5 μg/mL concentration but a significant difference was observed at ≥7.5 μg/mL (Figure 4D). At ≥7.5 μg/mL, the sensitivity of detection was between 85 and 95% while the specificity was from 60 to 70%.

Binding Characteristics of Antibodies on the Sensor. To understand the binding characteristics of RTO and KKO on the sensor, we immobilized PF4/H complexes on a gold surface and immobilized RTO or KKO on an AFM cantilever to measure the binding strength and to determine the binding kinetics of the interactions (Figure 5A, insert). When the cantilever approaches the substrate, the antibody interacts with the PF4/H complex, and their binding force (F) is detected when the cantilever ruptures from the substrate (inset, Figure 5A). By measuring 900 force−distance curves, collecting binding forces from different experiments in a histogram distribution, and fitting the data with a single Gaussian fit, the average ± SD of the binding force could be determined (Figure 5A). Our results showed that KKO binds to PF4/H complexes with a higher binding force than RTO, i.e., 31.5 ± 0.7 and 23.7 ± 0.2 pN, respectively.

As the binding force increases with the increase of pulling speed recorded by AFM, this relationship allows determination of the thermal off-rate k_{off} of the interaction by applying the Bell−Evans model.[48−50] The model describes that the rupture force increases proportionally to the natural logarithm of the loading rate ($\dot{F}$) (eq 3).

$$F(\dot{F}) = \frac{k_B T}{\Delta x} \ln\left(\frac{\dot{F}}{k_{off}} \times \frac{\Delta x}{k_B T}\right) \tag{3}$$

https://doi.org/10.1021/acsomega.1c02496
ACS Omega 2021, 6, 25926−25939

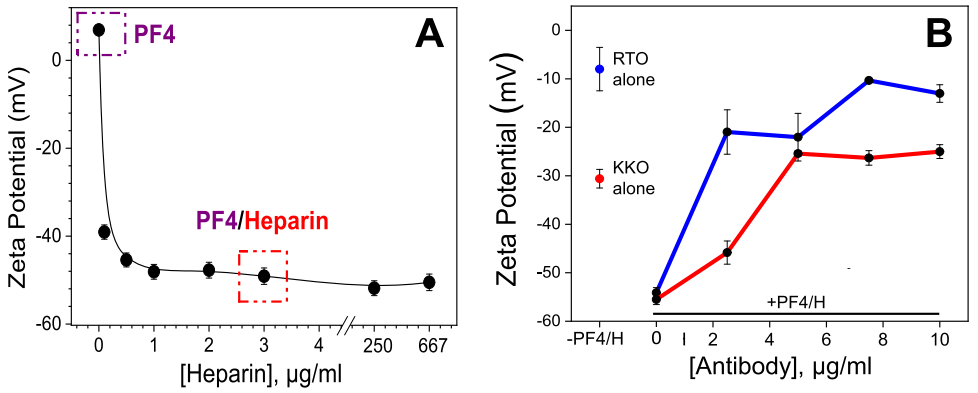

Figure 6. Zeta potential of proteins determined by DLS. (A) ζ potential of PF4 alone (violet) around +7 mV changed to approximately −40 mV after complexing with heparin (red) and further reduced to about −50 mV at higher heparin concentrations added. The red square showed the concentration used in EIS experiments. Without PF4/H, (B, left) RTO alone showed a lower negative ζ potential than KKO, while, in the presence of PF4/H (lines), KKO still showed a higher negative ζ potential compared to RTO at all concentrations up to 10 μg/mL.

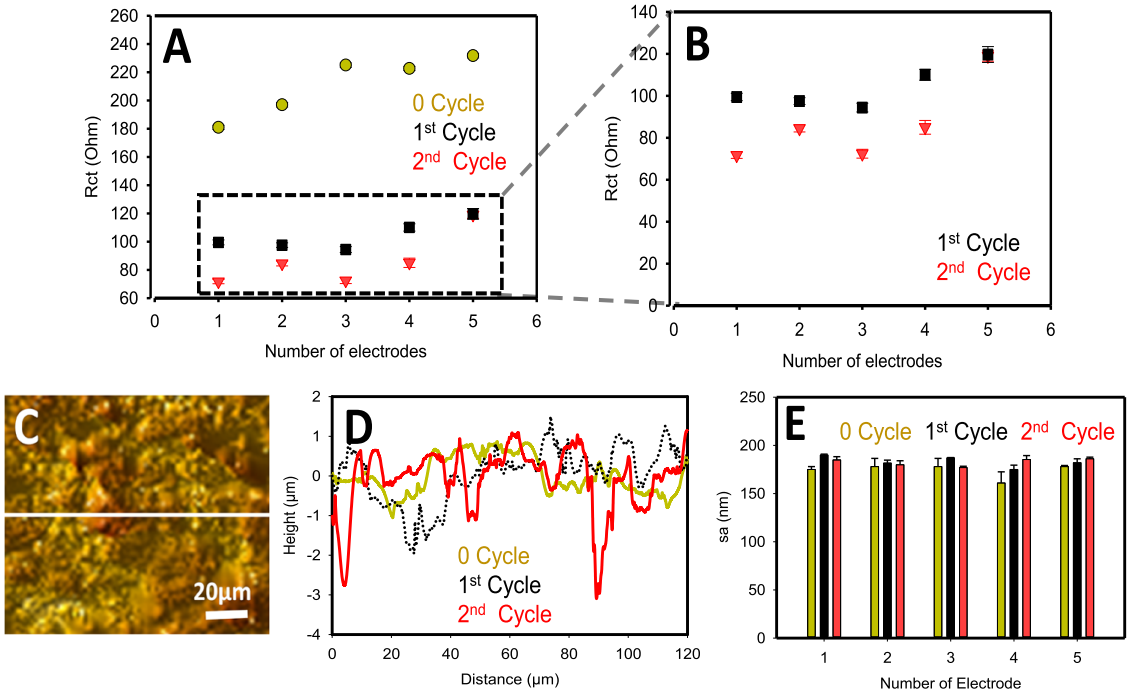

Figure 7. Characteristics of sensors after multiple uses. (A) R_{ct} changed after each wash cycle and was the highest for (yellow) the zero- (= new sensor), followed by the first (black), and the lowest for the second (red) washing cycle. (B) Enlargement of the R_{ct} for the first and second wash cycles. (C) Typical white light interferometry image of a sensor and line profile (white line) allowed us to obtain the roughness of the surface. (D) Line profiles show the variation of roughness after (yellow) zero-, (black dash) first, and (red) second washing cycles. (E) Average roughness (Sa) and SD obtained from different measurements for five electrodes showed a slight increase of roughness with increasing wash cycles but not for all electrodes; however, they were statistically not different as tested by one-way analysis of variance ($P > 0.06$).

where $\upsilon = \dot{F}/k_{eff}$, υ is the pulling speed and k_{eff} is the effective spring constant (composed of springs of the cantilever and antibody-PF4/H complexes); $\Delta x = k_BT/m$, where m is the slope of the fit, Δx is the distance from the bound to the unbound state, and $k_{off} = \dot{F}(F = 0)\ \Delta x/k_BT$ is the thermal off-rate of the interaction between the antibody and PF4/H complexes (eq 4)

$$\text{antibody} + \text{PF4/H} \underset{k_{off}}{\overset{k_{on}}{\rightleftarrows}} \text{antibody·PF4/H} \tag{4}$$

Here, we applied this method to identify the difference in the thermal off-rate between RTO and KKO. For this, binding forces were recorded at pulling speeds ranging from 0.5 to 7 μm/s and transferred to loading rates using JPK software based on the relation $\dot{F} = \upsilon k_{eff}$. The average values of forces at each speed and their corresponding SD are plotted in Figure 5B. Fitting the data allowed us to determine the slope and the relative thermal off-rates ($\sim k_{off}$) shown as the intercept at zero force. The calculated thermal off-rate induced by the bonds between RTO and PF4/H complexes is lower than that of KKO (Figure 5C), indicating a more stable binding of RTO than that of KKO. SMFS results showed a clear different binding characteristic between KKO and RTO.

Zeta Potential of Proteins. We suspect that the RTO and KKO differ not only in the binding strength and binding kinetics but also in the charge that resulted in different charge transfer resistances on the sensor. Thus, we next determined

https://doi.org/10.1021/acsomega.1c02496
ACS Omega 2021, 6, 25926−25939

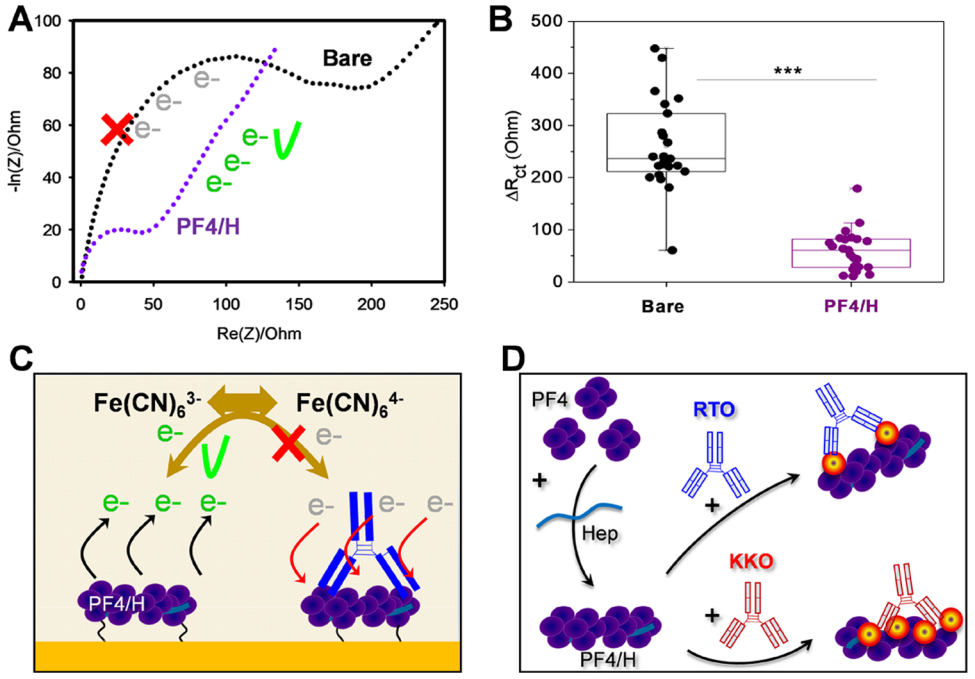

Figure 8. Binding characteristics of antibodies to PF4/Heparin complexes on the sensors. (A) Nyquist diagram showed a decrease in the charge transfer resistance after biding of PF4/H complexes (violet) compared to the bare chip (black). (B) Collection of R_{ct} measured with (black) bare electrodes and (violet) PF4/H-coated sensors. (C) Cartoons illustrate that the binding of PF4/H complexes along with ethanolamine promote charge transfer, while the bound antibody inhibited charge transfer in $Fe(CN)_6^{3-/4-}$. (D) RTO binds to only a single PF4 monomer, while KKO binds at the interface between two PF4 monomers, which belong to a PF4 tetramer.

the zeta (ζ) potential of the involved proteins including PF4, PF4/H complexes, RTO, and KKO in water (pH 6.7). PF4 alone shows a positive ζ potential of 6.9 ± 0.8 mV, whereas its complex with heparin turned to a negative ζ potential, which was further increased at higher heparin concentrations (Figure 6A). The PF4/H complexes prepared in EIS experiments showed a ζ potential of −49.1 ± 1.9 mV (red, Figure 6A). The negative ζ potential indicates that PF4/H complexes carry a highly negatively charged surface. When bound on the chip, the PF4/H complexes can therefore facilitate charge transfer that leads to a reduction of the resistance, as also described previously.[51,52]

In the absence of PF4/H, RTO also carries a negative charge surface but is weaker than KKO (Figure 6B, left boxes). In the presence of PF4/H, KKO up to 10 μg/mL showed a lower ζ potential compared to RTO (Figure 6B, lines). The difference in surface charges between RTO and KKO might relate to their dissimilar R_{ct} signals obtained on the sensor.

Lifetime of the Sensor. The lifetime of the sensor plays an important role in the usability application of the HIT antibody sensor. Therefore, we investigated the characteristics of the sensors after multiple usages or multiple washing cycles. We performed standard experiments as described above and then cleaned the sensors with a cleaning solution ($H_2O/H_2O_2/NH_3$, ratio 5:1:1) and reused them. We found a reduction in R_{ct} from the zero wash cycle (i.e., a new sensor) to the second wash cycle (Figure 7A,B). However, four among five electrodes showed only a slight decrease of R_{ct} after two wash cycles compared to the first wash cycle (Figure 7B). As more bound antibodies on the sensor will induce a higher R_{ct} value (Figure 5), the reduction of R_{ct} after the second wash cycle indicated a slight reduction of antibody binding as compared to that of the first wash cycle. To understand this change, we measured the roughness of the sensors by imaging the surfaces using white light interferometry (Figure 7C). Line profiles showed that the second wash cycle exhibited the highest depth, followed by the first wash cycle, and the lowest depth for the zero wash cycle. Average ± SD roughness of the whole surface showed a slight increase for later wash cycles (Figure 7C−E). Line profiles showed the highest depth for the second wash cycle, followed by the first wash cycle, and the lowest for the zero wash cycle. Probably, the cleaning solution etched the sensors that led to an increase of roughness and reduced the binding of biomolecules, and therefore, R_{ct} decreased. It is also possible that the gold layer was partially etched, leaving random surfaces without a gold layer for Au−thiol coupling, which limited the formation of the SAM layer for the linking of proteins. However, the changes are not significantly different as a minimal variation in R_{ct} was observed between the first and the second wash cycle. After the third and fourth washing cycles, further reduction of the R_{ct} signal was observed (data not shown). To minimize the effect of the washing cycle on the impedance signal, we used in this study, the sensors up to the second washing cycle.

DISCUSSION

In this study, we proved as a principle that the platelet-activating pathogenic HIT-like KKO antibody could be distinguished from the nonplatelet activating nonpathogenic HIT-like RTO antibody by electrochemical impedance spectroscopy (EIS). Furthermore, we provided an insight into the binding characteristics of these antibodies on the sensors.

The charge transfer resistance affected by the binding of RTO is significantly higher than that of KKO. The charge transfer resistance increased linearly as the antibody concentration increased. Fitting the data resulted in a clear difference in slopes between RTO and KKO (Figure 4A. The slope of

https://doi.org/10.1021/acsomega.1c02496
ACS Omega 2021, 6, 25926−25939

RTO is ∼6-fold higher than that of KKO, indicating a promising potential approach for future development of a sensor for distinguishing pathogenic aPF4/H Abs from nonpathogenic antibodies based on the valuation of slopes. However, large standard deviations of R_{ct} suggest that there is a need for improvement in the signal-to-noise ratio of this technique. The large standard deviation SD is attributed to the variation in the size of electrodes. To exclude this effect, we interpreted the signal ratio between bound antibodies and bound PF4/H complexes. This ratio indicated the signal of the antibody binding per PF4/H unit. The ratio interpretation revealed a better distinction between RTO and KKO at ≥7.5 μg/mL antibody concentrations.

Unlike many biomolecules binding to sensors that block charge transfer and lead to an increase of the charge transfer resistance (R_{ct}), binding of PF4/H complexes to the sensor reduced R_{ct}. A previous study showed that the reduction of R_{ct} is because the surface is doped with anions.[51,52] However, PF4 is a positively charged protein with a ζ potential of about +7 mV and the PF4 monomer has a molecular weight of 8 kDa but they mostly exist as a tetramer (32 kDa). The PF4 should behave similar to a cloud of cations instead of anions, which should result in an increase of R_{ct} instead of a decrease. Interestingly, when forming complexes with heparin, the resulting PF4/H complexes become highly negatively charged with a ζ potential of about −40 mV. It turns out that the PF4/H complexes behave like a cloud of anions that promote charge transfer or reduce resistance transfer as we observed a decrease in R_{ct} compared to that of bare electrodes (Figure 8A,B). However, binding of both KKO and RTO neutralize or block the surface charge of PF4/H complexes leading to an increase in R_{ct}. The R_{ct} further increases with increasing antibody concentrations, which is the general observation for binding of many other molecules on the sensors.[53,54] Our results showed that binding of PF4/H complexes to the sensor along with the addition of ethanolamine[55,56] promote charge transfer. We attribute that the sensor was doped with a combination of both negatively charged molecules (including hydroxyl groups after ethanolamine treatment and PF4/H complexes) and positively charged molecules (PF4 molecules which still exist inside the ultralarge PF4/H complexes). These together promote charge transfer or reduce resistance, while bound RTO or KKO antibodies on the sensors inhibited charge transfer in $Fe(CN)_6^{3-/4-}$ (Figure 8C). Higher R_{ct} caused by RTO than KKO indicates a higher density of bound RTO on the sensor that inhibited charge transfer. Consistently, immunofluorescence results also show higher binding of RTO than those of KKO. However, RTO showed lower mass deposition on the sensor than KKO. As KKO-PF4 showed about 10-fold higher on-rate than the RTO,[40] while QCM is a very sensitive method that can detect the mass change due to molecular interactions in real time, the higher on-rate of KKO results in more KKO molecules than that of RTO interacting with the antigens at the same time point. This caused a higher mass change for KKO than RTO.

The electrical signal obtained by EIS experiments is an unexpected observation as it has been shown that a single KKO molecule binds to PF4/H complexes with a stronger binding force than RTO.[40] The general sense for this is that the KKO should bind more stably to PF4/H complexes than RTO, but it was not obvious in our experiments. To understand the dissimilar behaviors between RTO and KKO on the sensor, we gained insights into molecular interactions by comparing their binding characteristics. Our measured binding forces are consistent with the previous studies[40] in which KKO interacted with PF4/H complexes with a higher force than RTO (Figure 5A). Surprisingly, a lower thermal off-rate (k_{off}) for RTO than for KKO was found, which indicates a more stable bond between RTO and PF4/H complexes compared to that of KKO. Consistently, KKO alone or in complex with PF4/H antigens exhibits a higher negative ζ potential than RTO (Figure 6B). Probably, the high negative charge surface of KKO repels the same negative charge surface of PF4/H complexes during binding, which leads to less stable bonds between KKO and the antigen. This repulsive force seems to be stronger than the interaction force caused by the binding of KKO in the open-end PF4 tetramer, which facilitated the dissociation of KKO from PF4/H complexes. In contrast, the repulsive force between RTO and PF4 is lower than that of KKO as RTO itself has a lower negative ζ potential than KKO. This leads to a more stable binding between RTO and PF4/H complexes than KKO. Our results indicated that not only specific binding but also the ζ potential of antibodies play a role in the stability (k_{off}) of antibodies to PF4/H complexes. The stable bonds facilitate RTO to bind on the sensor and inhibit charge transfer, whereas the less stable binding of KKO with a higher k_{off} value promotes it to dissociate from PF4/H complexes bound on sensors.

Even though these antibodies show different kinetic parameters, they both bind to PF4/H complexes as evident by different physical properties in other investigated platforms including QCM, CLSM, SMFS, and DLS. Interestingly, the difference in their binding kinetics could be electrically distinguished in EIS experiments, indicating the practicality of EIS in the detection of platelet-activating KKO antibodies. Besides, RTO binds on the surface of a single PF4 monomer, whereas KKO intercalates in between two PF4 monomers that belong to a single PF4 tetramer as a key−lock model (Figure 8D). This dissimilar binding structure may govern the affinity of these antibodies to the PF4/H complexes. As a result, RTO induced an overall higher charge transfer resistance R_{ct} than KKO.

Overall, based on different characteristics between HIT-like and non-HIT-like antibodies, they could be distinguished in EIS measurements. At ≥7.5 μg/mL, our EIS tests provide a sensitivity of detection between 85 and 95% while the specificity was from 60 to 70%. As the standard HIT ELISA has a sensitivity of ≥95% but only ∼50% specificity, EIS detection showed comparable sensitivity but better specificity for detection of HIT-like antibodies than that of ELISA. The stickiness of the PF4/H antigen coated on the sensor did not poison the sensor as we found that the sensor can be reused for at least two cycles.

RTO and KKO represent characteristics of human non-HIT anti-PF4/H antibodies and HIT anti-PF4/H antibodies, respectively. We recently found that the human anti-PF4/H antibodies isolated from HIT patients also showed different binding characteristics to PF4/H complexes including the binding force, binding energy, and thermal off-rate.[31] A group of patients contains anti-PF4/H antibodies that behave similar to RTO (which does not induce HIT), while another group of patients contains antibodies showing similar characteristics as KKO (which induces HIT). Interestingly, the group of patients containing noninducing HIT anti-PF4/H antibodies also shows a difference in the ζ potential and binding force as compared with the group of patients containing HIT anti-PF4/

https://doi.org/10.1021/acsomega.1c02496
ACS Omega 2021, 6, 25926−25939

H antibodies.[57] These two groups of patients show similar characteristics as RTO and KKO. Therefore, investigation using patient's sera may result in a potential application of EIS in the detection of HIT.

Available methods exhibit several limitations including high costs, long delay procedure for diagnosis, and delay in making a management decision for patients. Failure to diagnose HIT can lead to catastrophic thrombosis if heparin therapy is continued. Therefore, a quick and accurate diagnosis of HIT must be made in case it occurs, especially in Covid-19 infected patients or Covid-19 vaccinated individuals who suffer from side effects.[58] However, an effective method for the detection of HIT antibodies with high accuracy is still missing. A single assay that allows a rapid, reliable, and easy-to-test to reduce the overall costs and the patient's risk is highly expected. Our study opens an avenue for the detection of HIT antibodies by electrochemical impedance spectroscopy that is a noninvasive method without the requirement of a marker for detection and is a highly sensitive technique with detection limits as low as the picomolar range.[59] Impedance measurement of immunoreactions has been considered a plausible alternative method for immunological assays.[54] Application of EIS in detecting HIT antibodies may negate the lengthy and low accuracy in the current immunoassay/ELISAs as well as the high cost and requirement of fresh human blood in functional tests. Even though human sera contain multiple proteins that may affect EIS detection, our recent tests showed the same trend of changes in R_{ct} values when RTO or KKO were detected in the purified system or were mixed in sera of healthy donors (data not shown). The antibodies bind specifically to PF4/H complexes, while plasma proteins were thoroughly washed away as already established in the standard ELISA assays. However, further efforts including optimization of the SAM layer to minimize nonspecific binding as well as antigen and antibody concentrations, incubation time, detection buffer to gain the highest signal-to-noise ratio of detection are required.

CONCLUSIONS

As a proof of principle, we showed that a label-free biosensor for the detection of HIT-like KKO antibodies could be established based on electrochemical impedance spectroscopy. The non-HIT-like RTO exhibited a significantly higher charge transfer resistance than KKO that allowed us to differentiate them in EIS measurements. The distinction of electrical signals due to binding of these antibodies was characterized by complementary methodologies. The level of charge transfer resistance is governed by multiple factors such as the ζ potential of the involved proteins, binding strength/bond dynamics, and antigen−antibody binding structures. The stable bond of the RTO made it powerful in blocking charge transfer, whereas the less stable binding of KKO promoted charge transfer that allowed us to distinguish them in EIS experiments. Our study provides detailed binding characteristic differences between HIT-like and non-HIT-like antibodies, paving a way for future development of biosensors based on EIS for better detection of human HIT antibodies.

MATERIALS AND METHODS

Chemicals and Reagents. The following reagents were used: cysteamine-hydrochloride (Fluka, Sigma-Aldrich, 30080, Germany), ethanolamine (Sigma-Aldrich, E9508, Germany), glycine (Sigma-Aldrich, 092K0099, Germany), glutaraldehyde (Sigma-Aldrich grade I 25%), potassium-hexacyanoferrate (II) trihydrate (Merck, A870884, Darmstadt, Germany), potassium-hexacyanoferrate(III) trihydrate (Merck, A81167372124, Darmstadt, Germany), RTO and KKO (Invitrogen, Thermo Fisher, Germany), platelet factor 4 (Chromatec, Greifswald, Germany), UFH Heparin-Natrium-25000 (Ratiopharm, Ulm, Germany), and phosphate buffer saline (PBS) pH7.4. All of the chemicals were of the highest purity available and were used as purchased.

Quartz Crystal Microbalance (QCM). All preparations and experiments were done at room temperature (RT). A gold-coated quartz chip QSX 301 with a resonance frequency of 4.95 MHz ± 50 kHz (Biolin Scientific Darmstadt, Germany) was cleaned using a UV/ozone cleaner for 10 min and then dipped into a 5:1:1 mix of $H_2O/NH_3/H_2O_2$ in an ultrasonic bath for 10 min.[60,61] Then, the chip was rinsed with distilled water before drying with a nitrogen flow. After that, it was rinsed with ethanol and dried again under a nitrogen flow, as described by the Q-Sense "cleaning and immobilization protocols". The chip was then assembled in the chamber and connected to the pump (High Precision Multichannel Dispenser, ISMATEC) in the QCM instrument. To form a self-assembled monolayer (SAM) of cysteamine,[62] the chip was incubated immediately after cleaning with 5 mL of 30 mM cysteamine for 15 min, and then washed with 5 mL of water. A functional layer on cysteamine was generated by incubating in 5 mL of 30 mM glutaraldehyde. After washing with 1 mL of PBS, the chip was incubated with preformed PF4/H complexes composed of 20 μg/mL PF4 and 0.5 IU/mL UFH. After rinsing with PBS, 2 mL of 10 mM ethanolamine was added to block free aldehyde (−CHO) groups. Subsequently, 2.5 μg/mL RTO or KKO was added for binding with PF4/H complexes. QCM experiments were performed at a pumping speed of 100 μL/min with an incubation time of 6 min. In all experiments, only resonance mode of the QCM was used (Sense Analyzer, LOT Oriel Gruppe Europa). The change in resonant frequency was recorded at the third overtone due to stability constraints, a higher order. All QCM measurements were performed on Qsoft software (version 2.5.22.707, Q-Sense, Biolin Scientific, Europe). To obtain the deposition mass on the chip, data analysis was carried out using the Sauerbrey equation through Qtools software (version 3, Quantum Design, Darmstadt, Germany) and plotted using SigmaPlot (version 6).

Confocal Laser Scanning Microscopy (CLSM). Cleaning of the EIS sensor and coating of PF4/H complexes were performed using the same procedure as described above for QCM experiments. To confirm if PF4/H complexes were successfully immobilized on the sensor, an anti-PF4 FITC antibody (Dianova GmbH, Hamburg, Germany) of 20 μg/mL in PBS was added to the chip coated with PF4/H complexes and incubated for 30 min in the dark. To bind antibodies to PF4/H complex-coated sensors, RTO or KKO (10 μg/mL) was added and incubated on each sensor for 1h. The successful binding of antibodies on the chip was examined by immunofluorescence tests. For that, the chip was then incubated with anti-mouse IgG Alexa 488 (Abcam, Cambridge, U.K.) of 2 μg/mL in PBS for 30 min in the dark. Unbound antibodies were removed by rinsing with PBS. Samples were examined with a confocal laser scanning microscope Zeiss LSM710 (Carl Zeiss, Gottingen, Germany). ImageJ software was used to further process the images and to quantify the fluorescence intensity detected on each sample (open source).

https://doi.org/10.1021/acsomega.1c02496
ACS Omega 2021, 6, 25926−25939

Electrochemical Impedance Spectroscopy (EIS). The sensor was gold (Au DuPont 5771) on an alumina substrate with an aluminum binder in between made by screen printing (Micro-Hybrid, Hermsdorf, Germany). The sensor consists of six electrodes where the first five electrodes are of the same size and were used in this study, while the sixth electrode is larger and was excluded.

The EIS sensors were cleaned using the same procedure as described above for the QCM experiments. Subsequently, an additional cleaning step using cyclic voltammetry (CV) with sweeping the potential in the range of −0.4 to 1.0 V and at a scan rate of 100 mV/s in PBS was performed. Immobilization of proteins on the EIS sensor is followed by the same protocol as described in the QCM section including (i) coating with the SAM layer, (ii) immobilization of PF4/H complexes, and (iii) pumping RTO and KKO through the sensors for binding. The chip was then placed into the measurement chamber holding a platinum counter electrode and Ag/AgCl reference electrode (Xylem, Waldheim, Germany). The RTO or KKO antibodies of different concentrations of 0, 2.5, 5.0, 7.5, and 10.0 μg/mL were pumped at a flow rate of 100 μL/mL through the chamber using a peristaltic pump (IPC-16, Ismatec, Cole−Parmer GmbH, Wertheim, Germany). Human control antibodies in sera that do not bind to PF4/H complexes in ELISA and do not induce platelet activation were used as the control. The serum was heated at 37 °C for 5 min and a 1:200 dilution following the standard protocol in ELISA was tested. All fluidic connections were made with a Teflon tube of a 0.5 mm inner diameter. Each antibody concentration was pumped through the chamber for 6 min of incubation with the subsequent impedance measurement. After that, bound antibodies on the sensor were removed by pumping 1 mL of glycine 100 mM. This process was repeated with the dilution series of both antibodies. The electrolyte solution used for measurement was 4 mM ferri-/ferrocyanide.

The impedance was measured using an SP-150 Bio-Logic impedance analyzer and recorded with EC-Lab (version 11.34, Bio-Logic Science Instruments SAS, Claix, France). The frequency range was 1 Hz to 100 kHz with logarithmic spacing and a sinusoidal voltage of 10 mV. The analysis and fitting were done with the Z-fit analysis tool integrated into the EC-Lab program, SigmaPlot (version 6), and Origin software (version 7.5).

Single-Molecule Force Spectroscopy (SMFS). SMFS experiments were performed to determine the binding strength and thermal kinetics of the bond between RTO or KKO and PF4/H complexes, as previously[31−34] described. Briefly, a gold-coated silicon nitride cantilever with a nominal spring constant of 6 pN/nm or 30 pN/nm (Olympus Biolever, Tokyo, Japan) was coated with thiol-PEG-COOH (3400 Da, Nanocs). After that, the −COOH groups at the end of PEG linkers were activated with an amine coupling kit (Biacore, Uppsala, Sweden), containing a mixture of 0.4 M 1-ethyl-3-(3-dimethyl aminopropyl) carbodiimide hydrochloride (EDC) and 0.1 M *N*-hydroxy succinimide (NHS) for binding of proteins.[63,64] RTO or KKO with a concentration of 70 μg/mL was applied to the cantilevers for 30 min at RT and then kept overnight at 4 °C. After rinsing the unbound antibodies, free activated groups on the surfaces were blocked by adding 1.0 M ethanolamine (GE Healthcare, Uppsala, Sweden) for 1 h at RT.

PF4/H complexes were immobilized on gold-coated glass with the same protocol as used for coating antibodies on the cantilever. PF4/H complexes were preformed by a mixture of 20 μg/mL PF4 with 0.5 IU/mL heparin (Heparin-Natrium-25 000, Ratiopharm GmbH, Ulm, Germany) in PBS for 1 h at RT. For immobilization, PF4/H complexes were kept on the $^{-}$OOC-PEG-coated Au surfaces at RT for 30 min and then overnight at 4 °C.

The SMFS measurements were carried out in PBS using JPK NanoWizard 3 (Berlin, Germany) with a setpoint of 200 pN and 900 force−distance (F−D) curves per condition. The thermal off-rates (k_{off}) which is the dissociation constant of the bonds between antibodies and PF4/H complexes were determined by applying the Bell−Evans model to the relation between loading rates and rupture forces,[48−50] which were measured at pull-off speeds ranging from 0.5 to 7 μm/s. JPK data processing software (version 4.4.18+, JPK, Berlin, Germany) was used to analyze the measured adhesion forces and to determine the loading rates. The mean rupture force values and their corresponding errors were determined by applying Gaussian fits to the data using Origin software (version 9.1) and SigmaPlot (version 6).

Zeta Potential. To determine the surface ζ potential of PF4 or RTO or KKO or RTO and KKO when binding to PF4/H complexes, 0.9 mL of protein at a concentration of 20 μg/mL PF4 or PF4/H complexes in water (pH 6.7) was loaded into a folded capillary zeta cell and measured before titrating the antibody concentration up to 10 μg/mL. The migration speed in an electric field was assessed using dynamic light scattering at a fixed angle (173°) with the Zetasizer Nano-S system (Malvern Instruments Ltd., Malvern, U.K.). The measurements were performed at 25 °C using 6−10 repeating measurements. Data analysis was performed using Zetasizer software, version 7.11 (Malvern Instruments Ltd., Malvern, U.K.) and Origin software, version 7.5.

White Light Interferometry (WLI). The sensors from EIS experiments were cleaned in the cleaning ($H_2O/H_2O_2/NH_3$, ratio 5:1:1) solution after each usage and their surface topography was imaged. The surface roughness of the sensors was measured with WLI using a Bruker contour GTK-3D (Bruker Nano GmbH, Berlin) with an optical microscope and vertical scanning option of 50× magnification, a measurement area of X = 125.8 μm and Y = 94.8 μm, and a lateral resolution of 640 × 480 pixel^2. The images were further analyzed with SPIP (version, 6.6.5, Image Metrology, Denmark). A global tilt compensation and a filter wavelength of an ISO 16610 Gaussian L filter 1/7 of the lateral measurement dimensions were applied according to ISO 25178-2 to remove form and waviness and to calculate the average whole surface roughness (Sa). The roughness obtained was taken from three points on each electrode up to the second washing cycle and was averaged.

AUTHOR INFORMATION

Corresponding Author

Thi-Huong Nguyen − *Institute for Bioprocessing and Analytical Measurement Techniques (iba), 37308 Heiligenstadt, Germany; Institute for Chemistry and Biotechnology, Faculty of Mathematics and Natural Sciences, Technische Universität Ilmenau, 98694 Ilmenau, Germany;* orcid.org/0000-0002-9237-3482; Email: thi-huong.nguyen@iba-heiligenstadt.de

https://doi.org/10.1021/acsomega.1c02496
ACS Omega 2021, 6, 25926−25939

Authors

Nida Zaman Khan − *Institute for Bioprocessing and Analytical Measurement Techniques (iba), 37308 Heiligenstadt, Germany; Institute for Chemistry and Biotechnology, Faculty of Mathematics and Natural Sciences, Technische Universität Ilmenau, 98694 Ilmenau, Germany*

Li-Yu Chen − *Institute for Bioprocessing and Analytical Measurement Techniques (iba), 37308 Heiligenstadt, Germany; Institute of Microbiology, Friedrich Schiller University, 07745 Jena, Germany*

Annerose Lindenbauer − *Institute for Bioprocessing and Analytical Measurement Techniques (iba), 37308 Heiligenstadt, Germany*

Uwe Pliquett − *Institute for Bioprocessing and Analytical Measurement Techniques (iba), 37308 Heiligenstadt, Germany*

Holger Rothe − *Institute for Bioprocessing and Analytical Measurement Techniques (iba), 37308 Heiligenstadt, Germany*

Complete contact information is available at: https://pubs.acs.org/10.1021/acsomega.1c02496

Author Contributions

N.Z.K. and L.-Y.C. contributed equally to this work. N.Z.K. performed and analyzed the data from EIS, QCM, DLS, and WLI experiments and wrote the manuscript. L.-Y.C. prepared and carried out SMFS and CLSM experiments, analyzed results, and wrote the manuscript. U.P. discussed EIS and QCM results. H.R. supported with WLI experiments and analysis. A.L. performed DLS experiments. T.-H.N. conceived the project, analyzed the data, and wrote the manuscript. All authors agreed with the final version of the manuscript.

Notes

The authors declare no competing financial interest.

■ ACKNOWLEDGMENTS

This work was supported by the Freistaat Thüringen, Germany and the Deutsche Forschungsgemeinschaft (DFG, Germany, Project number: NG 133/1-2). We thank Dieter Frense for his support with EIS and QCM experiments, Uwe Schrimer and Katharina Schieke for their technical support with QCM experiments, and Prof. Dr. Doris Heinrich for revising our manuscript.

■ REFERENCES

(1) Linhardt, R. J. 2003 Claude S. Hudson Award Address in Carbohydrate Chemistry. Heparin: Structure and Activity. *J. Med. Chem.* **2003**, *46*, 2551−2564.

(2) Kern, A.; Schmidt, K.; Leder, C.; Müller, O. J.; Wobus, C. E.; Bettinger, K.; Von der Lieth, C. W.; King, J. A.; Kleinschmidt, J. A. Identification of a heparin-binding motif on adeno-associated virus type 2 capsids. *J. Virol.* **2003**, *77*, 11072−11081.

(3) Linder, A.; Soehnlein, O.; Åkesson, P. Roles of Heparin-Binding Protein in Bacterial Infections. *J. Innate Immun.* **2010**, *2*, 431−438.

(4) Rak, J.; Weitz, J. I. Heparin and angiogenesis: size matters! *Arterioscler. Thromb. Vasc. Biol.* **2003**, *23*, 1954−1955.

(5) Wang, L.; Brown, J. R.; Varki, A.; Esko, J. D. Heparin's anti-inflammatory effects require glucosamine 6-O-sulfation and are mediated by blockade of L- and P-selectins. *J. Clin. Invest.* **2002**, *110*, 127−136.

(6) LAZO-LANGNER, A.; GOSS, G. D.; SPAANS, J. N.; RODGER, M. A. The effect of low-molecular-weight heparin on cancer survival. A systematic review and meta-analysis of randomized trials. *J. Thromb. Haemost.* **2007**, *5*, 729−737.

(7) Oduah, E. I.; Linhardt, R. J.; Sharfstein, S. T. Heparin: Past, Present, and Future. *Pharmaceuticals* **2016**, *9*, No. 38.

(8) Greinacher, A. CLINICAL PRACTICE. Heparin-Induced Thrombocytopenia. *N. Engl. J. Med.* **2015**, *373*, 252−261.

(9) Khandelwal, S.; Arepally, G. M. Immune pathogenesis of heparin-induced thrombocytopenia. *Thromb. Haemost.* **2016**, *116*, 792−798.

(10) Cai, Z.; Yarovoi, S. V.; Zhu, Z.; Rauova, L.; Hayes, V.; Lebedeva, T.; Liu, Q.; Poncz, M.; Arepally, G.; Cines, D. B.; Greene, M. I. Atomic description of the immune complex involved in heparin-induced thrombocytopenia. *Nat. Commun.* **2015**, *6*, No. 8277.

(11) Fathi, M. Heparin-induced thrombocytopenia (HIT): Identification and treatment pathways. *Glob. Cardiol. Sci. Pract.* **2018**, *2018*, No. 15.

(12) Ahmed, I.; Majeed, A.; Powell, R. Heparin induced thrombocytopenia: diagnosis and management update. *Postgrad. Med. J.* **2007**, *83*, 575−582.

(13) Cummins, D.; Halil, O.; Amin, S. Which patients undergoing cardiopulmonary bypass should be assessed for development of heparin-induced thrombocytopenia? *Thromb. Haemost.* **1995**, *73*, 890.

(14) Go, A. S.; Mozaffarian, D.; Roger, V. L.; Benjamin, E. J.; Berry, J. D.; Borden, W. B.; Bravata, D. M.; Dai, S.; Ford, E. S.; Fox, C. S.; Franco, S.; Fullerton, H. J.; Gillespie, C.; Hailpern, S. M.; Heit, J. A.; Howard, V. J.; Huffman, M. D.; Kissela, B. M.; Kittner, S. J.; Lackland, D. T.; Lichtman, J. H.; Lisabeth, L. D.; Magid, D.; Marcus, G. M.; Marelli, A.; Matchar, D. B.; McGuire, D. K.; Mohler, E. R.; Moy, C. S.; Mussolino, M. E.; Nichol, G.; Paynter, N. P.; Schreiner, P. J.; Sorlie, P. D.; Stein, J.; Turan, T. N.; Virani, S. S.; Wong, N. D.; Woo, D.; Turner, M. B.; American Heart Association Statistics Committee and Stroke Statistics Subcommittee. Heart disease and stroke statistics–2013 update: a report from the American Heart Association. *Circulation* **2013**, *127*, e6−e245.

(15) Thachil, J.; Tang, N.; Gando, S.; Falanga, A.; Cattaneo, M.; Levi, M.; Clark, C.; Iba, T. ISTH interim guidance on recognition and management of coagulopathy in COVID-19. *J. Thromb. Haemost.* **2020**, *18*, 1023−1026.

(16) Tang, N.; Bai, H.; Chen, X.; Gong, J.; Li, D.; Sun, Z. Anticoagulant treatment is associated with decreased mortality in severe coronavirus disease 2019 patients with coagulopathy. *J. Thromb. Haemost.* **2020**, *18*, 1094−1099.

(17) Yin, S.; Huang, M.; Li, D.; Tang, N. Difference of coagulation features between severe pneumonia induced by SARS-CoV2 and non-SARS-CoV2. *J. Thromb. Thrombolysis* **2021**, *51*, 1107−1110.

(18) Dragonetti, D.; Guarini, G.; Pizzuti, M. Detection of anti-heparin-PF4 complex antibodies in COVID-19 patients on heparin therapy. *Blood Transfus.* **2020**, *18*, No. 328.

(19) Althaus, K.; Marini, I.; Zlamal, J.; Pelzl, L.; Singh, A.; Haberle, H.; Mehrlander, M.; Hammer, S.; Schulze, H.; Bitzer, M.; Malek, N.; Rath, D.; Bosmuller, H.; Nieswandt, B.; Gawaz, M.; Bakchoul, T.; Rosenberger, P. Antibody-induced procoagulant platelets in severe COVID-19 infection. *Blood* **2021**, *137*, 1061−1071.

(20) Zuo, Y.; Estes, S. K.; Ali, R. A.; Gandhi, A. A.; Yalavarthi, S.; Shi, H.; Sule, G.; Gockman, K.; Madison, J. A.; Zuo, M.; Yadav, V.; Wang, J.; Woodard, W.; Lezak, S. P.; Lugogo, N. L.; Smith, S. A.; Morrissey, J. H.; Kanthi, Y.; Knight, J. S. Prothrombotic autoantibodies in serum from patients hospitalized with COVID-19. *Sci. Transl. Med.* **2020**, *12* (570), No. eabd3876.

(21) Chan, M.; Malynn, E.; Shaz, B.; Uhl, L. Utility of consecutive repeat HIT ELISA testing for heparin-induced thrombocytopenia. *Am. J. Hematol.* **2008**, *83*, 212−217.

(22) Smythe, M. A.; Warkentin, T. E.; Woodhouse, A. L.; Zakalik, D. Venous limb gangrene and fatal hemorrhage: adverse consequences of HIT "overdiagnosis" in a patient with antiphospholipid syndrome. *Am. J. Hematol.* **2011**, *86*, 188−191.

(23) Warkentin, T. E. Laboratory testing for heparin-induced thrombocytopenia. *J. Thromb. Thrombolys* **2000**, *10*, S35−S45.

(24) Greinacher, A.; Amiral, J.; Dummel, V.; Vissac, A.; Kiefel, V.; Muellereckhardt, C. Laboratory Diagnosis of Heparin-Associated Thrombocytopenia and Comparison of Platelet-Aggregation Test,

Heparin-Induced Platelet Activation Test, and Platelet Factor-4 Heparin Enzyme-Linked-Immunosorbent-Assay. *Transfusion* **1994**, *34*, 381−385.
(25) WARKENTIN, T. E.; SHEPPARD, J. I.; RASCHKE, R.; GREINACHER, A. Performance characteristics of a rapid assay for anti-PF4/heparin antibodies: the particle immunofiltration assay. *J. Thromb. Haemost.* **2007**, *5*, 2308−2310.
(26) Nagler, M.; Bachmann, L. M.; ten Cate, H.; ten Cate-Hoek, A. Diagnostic value of immunoassays for heparin-induced thrombocytopenia: a systematic review and meta-analysis. *Blood* **2016**, *127*, 546−557.
(27) Sachs, U. J.; von Hesberg, J.; Santoso, S.; Bein, G.; Bakchoul, T. Evaluation of a new nanoparticle-based lateral-flow immunoassay for the exclusion of heparin-induced thrombocytopenia (HIT). *Thromb. Haemost.* **2011**, *106*, 1197−202.
(28) Bankova, A.; Andres, Y.; Horn, M. P.; Alberio, L.; Nagler, M. Rapid immunoassays for diagnosis of heparin-induced thrombocytopenia: Comparison of diagnostic accuracy, reproducibility, and costs in clinical practice. *PLoS One* **2017**, *12*, e0178289.
(29) Hussain, M.; Northoff, H.; Gehring, F. Detection of HIT antibody dependent aggregation using novel surface imprinting approach. *Talanta* **2016**, *147*, 1−7.
(30) Morel-Kopp, M. C.; Aboud, M.; Tan, C. W.; Kulathilake, C.; Ward, C. Whole blood impedance aggregometry detects heparin-induced thrombocytopenia antibodies. *Thromb. Res.* **2010**, *125*, e234−e239.
(31) Nguyen, T. H.; Medvedev, N.; Delcea, M.; Greinacher, A. Anti-platelet factor 4/polyanion antibodies mediate a new mechanism of autoimmunity. *Nat. Commun.* **2017**, *8*, No. 14945.
(32) Nguyen, T. H.; Greinacher, A. Platelet factor 4/heparin complexes present epitopes differently on solid-phase vs platelet surfaces. *Blood* **2017**, *129*, 3498−3501.
(33) Nguyen, T. H.; Greinacher, A. Effect of pH and ionic strength on the binding strength of anti-PF4/polyanion antibodies. *Eur. Biophys. J.* **2017**, *46*, 795−801.
(34) Nguyen, T. H.; Greinacher, A. Distinct Binding Characteristics of Pathogenic Anti-Platelet Factor-4/Polyanion Antibodies to Antigens Coated on Different Substrates: A Perspective on Clinical Application. *ACS Nano* **2018**, *12*, 12030−12041.
(35) Casuso, I.; Rico, F.; Scheuring, S. Biological AFM: where we come from–where we are–where we may go. *J. Mol. Recognit.* **2011**, *24*, 406−413.
(36) Bui, V.-C.; Nguyen, T. H. The Role of Single-Molecule Force Spectroscopy in Unraveling Typical and Autoimmune Heparin-induced Thrombocytopenia. *Int. J. Mol. Sci.* **2018**, *19*, No. 1054.
(37) Müller, D. J.; Helenius, J.; Alsteens, D.; Dufrêne, Y. F. Force probing surfaces of living cells to molecular resolution. *Nat. Chem. Biol.* **2009**, *5*, 383−390.
(38) Bahadır, E. B.; Sezgintürk, M. K. A review on impedimetric biosensors. *Artif. Cells Nanomed. Biotechnol.* **2016**, *44*, 248−262.
(39) Silva, M.; Helali, S.; Esseghaier, C.; Suarez, C.; Oliva, A.; Abdelghani, A. An impedance spectroscopy method for the detection and evaluation of Babesia bovis antibodies in cattle. *Sens. Actuators, B* **2008**, *135*, 206−213.
(40) Sachais, B. S.; Litvinov, R. I.; Yarovoi, S. V.; Rauova, L.; Hinds, J. L.; Rux, A. H.; Arepally, G. M.; Poncz, M.; Cuker, A.; Weisel, J. W.; Cines, D. B. Dynamic antibody-binding properties in the pathogenesis of HIT. *Blood* **2012**, *120*, 1137−1142.
(41) Rauova, L.; Zhai, L.; Kowalska, M. A.; Arepally, G. M.; Cines, D. B.; Poncz, M. Role of platelet surface PF4 antigenic complexes in heparin-induced thrombocytopenia pathogenesis: diagnostic and therapeutic implications. *Blood* **2006**, *107*, 2346−2353.
(42) Althaus, K.; Hron, G.; Strobel, U.; Abbate, R.; Rogolino, A.; Davidson, S.; Greinacher, A.; Bakchoul, T. Evaluation of automated immunoassays in the diagnosis of heparin induced thrombocytopenia. *Thromb. Res.* **2013**, *131*, e85−e90.
(43) Jourdy, Y.; Nougier, C.; Rugeri, L.; Bordet, J. C.; Sobas, F.; Negrier, C. Prospective evaluation of automatized PF4/heparin immunoassays HemosIL HIT-ab (PF4-H) for the diagnosis of heparin-induced thrombocytopenia. *Int. J. Lab. Hematol.* **2015**, *37*, 244−252.
(44) Yagati, A. K.; Chavan, S. G.; Baek, C.; Lee, M.-H.; Min, J. Label-Free Impedance Sensing of Aflatoxin B1 with Polyaniline Nanofibers/Au Nanoparticle Electrode Array. *Sensors* **2018**, *18*, 1320.
(45) Sauerbrey, G. Use of quartz vibration for weighing thin films on a microbalance. *J. Phys.* **1959**, *155*, 206−222.
(46) Brandt, S.; Krauel, K.; Gottschalk, K. E.; Renne, T.; Helm, C. A.; Greinacher, A.; Block, S. Characterisation of the conformational changes in platelet factor 4 induced by polyanions: towards in vitro prediction of antigenicity. *Thromb. Haemost.* **2014**, *112*, 53−64.
(47) Kreimann, M.; Brandt, S.; Krauel, K.; Block, S.; Helm, C. A.; Weitschies, W.; Greinacher, A.; Delcea, M. Binding of anti-platelet factor 4/heparin antibodies depends on the thermodynamics of conformational changes in platelet factor 4. *Blood* **2014**, *124*, 2442−2449.
(48) Merkel, R.; Nassoy, P.; Leung, A.; Ritchie, K.; Evans, E. Energy landscapes of receptor-ligand bonds explored with dynamic force spectroscopy. *Nature* **1999**, *397*, 50−53.
(49) Evans, E. Probing the Relation Between Force—Lifetime—and Chemistry in Single Molecular Bonds. *Annu. Rev. Biophys. Biomol. Struct.* **2001**, *30*, 105−128.
(50) Evans, E.; Leung, A.; Hammer, D.; Simon, S. Chemically distinct transition states govern rapid dissociation of single L-selectin bonds under force. *Proc. Natl. Acad. Sci. U.S.A.* **2001**, *98*, 3784−3789.
(51) Luo, Y.-z.; He, L.-h.; Liu, X.-h. Effect of Mg doping on electrochemical performance of Li3V2(PO4)3/C cathode material for lithium ion batteries. *Trans. Nonferrous Met. Soc. China* **2015**, *25*, 2266−2271.
(52) Badea, M.; Floroian, L.; Restani, P.; Cobzac, S. C. A.; Moga, M. Ochratoxin A Detection on Antibody- Immobilized on BSA-Functionalized Gold Electrodes. *PLoS One* **2016**, *11*, No. e0160021.
(53) Chornokur, G.; Arya, S. K.; Phelan, C.; Tanner, R.; Bhansali, S. Impedance-Based Miniaturized Biosensor for Ultrasensitive and Fast Prostate-Specific Antigen Detection. *J. Sens.* **2011**, *2011*, 1−7.
(54) Park, J. S.; Kim, H. J.; Lee, J.-H.; Park, J. H.; Kim, J.; Hwang, K. S.; Lee, B. C. Amyloid Beta Detection by Faradaic Electrochemical Impedance Spectroscopy Using Interdigitated Microelectrodes. *Sensors* **2018**, *18*, No. 426.
(55) Trzeciakiewicz, H.; Esteves-Villanueva, J.; Soudy, R.; Kaur, K.; Martic-Milne, S. Electrochemical Characterization of Protein Adsorption onto YNGRT-Au and VLGXE-Au Surfaces. *Sensors* **2015**, *15*, 19429−19442.
(56) Malvano, F.; Albanese, D.; Crescitelli, A.; Pilloton, R.; Esposito, E. Impedimetric Label-Free Immunosensor on Disposable Modified Screen-Printed Electrodes for Ochratoxin A. *Biosensors* **2016**, *6*, No. 33.
(57) Vayne, C.; Nguyen, T. H.; Rollin, J.; Charuel, N.; Poupon, A.; Pouplard, C.; Normann, N.; Gruel, Y.; Greinacher, A. Characterization of New Monoclonal PF4-Specific Antibodies as Useful Tools for Studies on Typical and Autoimmune Heparin-Induced Thrombocytopenia. *Thromb. Haemost.* **2021**, *121*, 322−331.
(58) Greinacher, A.; Thiele, T.; Warkentin, T. E.; Weisser, K.; Kyrle, P. A.; Eichinger, S. Thrombotic Thrombocytopenia after ChAdOx1 nCov-19 Vaccination. *N. Engl. J. Med.* **2021**, *384*, 2092−2101.
(59) Narakathu, B.; Guo, W.; Obare, S.; Atashbar, M. Detection of Picomolar Levels of Toxic Organophosphorus Compounds by Electrochemical and Fluorescence Spectroscopy. *Sens. Lett.* **2011**, *9*, 907−909.
(60) Li, X.; Wu, X.; Shi, P.; Ye, Z.-G. Lead-Free Piezoelectric Diaphragm Biosensors Based on Micro-Machining Technology and Chemical Solution Deposition. *Sensors* **2016**, *16*, 69.
(61) Zhao, B.; Hu, J.; Ren, W.; Xu, F.; Wu, X.; Shi, P.; Ye, Z.-G. A new biosensor based on PVDF film for detection of nucleic acids. *Ceram. Int.* **2015**, *41*, S602−S606.
(62) Wirde, M.; Gelius, U.; Nyholm, L. Self-Assembled Monolayers of Cystamine and Cysteamine on Gold Studied by XPS and Voltammetry. *Langmuir* **1999**, *15*, 6370−6378.

https://doi.org/10.1021/acsomega.1c02496
ACS Omega 2021, 6, 25926−25939

(63) Nguyen, T.-H.; Greinacher, A.; Delcea, M. Quantitative description of thermodynamic and kinetic properties of the platelet factor 4/heparin bonds. *Nanoscale* **2015**, *7*, 10130−10139.
(64) Nguyen, T.-H.; Steinbock, L. J.; Butt, H.-J.; Helm, M.; Berger, R. Measuring single small molecule binding via rupture forces of a split aptamer. *J. Am. Chem. Soc.* **2011**, *133*, 2025−2027.

https://doi.org/10.1021/acsomega.1c02496
ACS Omega 2021, 6, 25926−25939